Research Article

Lightweight Design and Dynamics Analysis of ZYL-15000D Directional Drill Reducer

Xiaohong Zhao [iD],[1,2] **Xianguo Yan** [iD],[1] **Zhi Chen** [iD],[1] and **Hang Su** [iD][1]

[1]*School of Mechanical Engineering, Taiyuan University of Science and Technology, Taiyuan 030024, China*
[2]*Fengtai Locomotive Depot, China Railway Beijing Bureau Group Co. LTD., Beijing 100070, China*

Correspondence should be addressed to Xianguo Yan; yan_xg2008@126.com

Since the output torque of the rotary reducer of the ZYL-15000D-kilometer directional drill is proportional to the gear train transmission ratio, the output torque is large enough when the input speed and output speed meet the design goal. This paper selects the method of reducing the transmission ratio to optimize the size parameters of the reducer. MATLAB genetic algorithm is used in the optimization design, and the minimum volume of the rotary part reducer is taken as the objective of optimization design, while the design variables and constraints are determined. The optimal value of design variables was obtained through optimization, and the parameter values of each gear were determined accordingly. Through analysis, the total volume of the optimized gear reducer was reduced by 49.6%. Then, the 3D model of the optimized gear was created, and the analysis of the transient dynamics of the optimized gear was carried out with ANSYS Workbench software. According to the analysis results, the optimized gear met the strength requirements and provided a reference for the subsequent optimization design of other types of gear reducers.

1. Introduction

Horizontal directional drilling is a trenchless construction method, which is usually completed by directional drilling RIGS, steering bits, and steering instruments [1]. The steps of the directional drill include drilling along the design path, reaming with a reamer, and pulling back of the product or casing [2, 3].

Directional drilling technology is not only used in pipeline laying and geological exploration but more importantly in coal mine gas drainage and discharge operations. It is the key technology of coal mine gas control and can ensure efficient extraction and safe production of coal, so it has been listed as a key development direction in the national coal industry "The Thirteenth Five-Year" development plan [2, 4–7].

The horizontal directional drilling machine is a piece of special equipment for underground gas extraction. It is a directional drilling technology with a screw motor with a bent joint. A screw motor is a kind of bottom-hole dynamic drilling tool with high-pressure washing fluid as the transmission power medium. It adopts screw drilling tools with different forms of deflecting parts and is equipped with measuring instruments while drilling, electrical control system, etc., which can flexibly meet the directional drilling needs of different design requirements [1, 8]. The reducer drives the power head to realize the all-round operation of the roadway. Due to the environmental characteristics of narrow roadway in coal mine, the drilling rig must be convenient for installation and disassembly. Therefore, under the condition of meeting the requirements of working conditions, it is very important to optimize the design of reducer [9]. The object of this paper is the reducer of the rotary part of ZYL-15000D horizontal directional drill. Taking the minimum volume of reducer as the optimization design goal, the mathematical model of the optimization

design of directional drill reducer was established, including the objective function, design variables, and constraints. MATLAB software is used to the optimization design based on genetic algorithm, and the optimization results were obtained [10–12]. Creo was used to model the optimized gear to obtain the 3D model of the gear. Then, the 3D gear model was imported into ANSYS Workbench to perform transient dynamics analysis on the gear to verify the reliability of the optimized model [13–15].

2. Structural Analysis of Reducer

Figure 1 shows the simplified transmission diagram of the reduction box of the rotary part of the drill. The overall structure is divided into two stages of reduction. The first stage of reduction involves the planetary gear system, and the second stage of reduction involves the helical gear group driven by the planetary frame. The gear parameters of the original gearbox are shown in Table 1.

To facilitate the analysis of this optimization calculation, the whole gear train is divided into three zones: planetary gears A and B and helical gears.

Because the transmission structure and transmission mode of planetary gears A and B are consistent, the calculation is mainly carried out by planetary gear train A and helical gear set.

3. Mathematical Model of Reducer Optimization Design

Genetic algorithm (GA) is an algorithm that simulates the evolution of organisms by computer based on the genetic characteristics of organisms; the general steps of genetic algorithm are as follows: first replace the feasible solution with chromosomes, and these produced chromosomes are called feasible solution set. Then, the chromosome is put into "nature" according to the law of biological evolution in nature, excellent individuals are selected for crossover and mutation, and new chromosome individuals are produced. After several times of screening, the optimal individual is finally converged according to the conditions, and the genetic algorithm completes the optimization [16–18].

MATLAB genetic algorithm toolbox provides two methods; the two methods are command line call GA function and graphical user interface. The GUI method only needs to input the number of variables, the upper and lower limits of constraint values, the M file name of the prepared fitness function, and the M file name of the constraint function on the interface and set the population size, crossover probability, and mutation probability of the optional parameters to carry out optimization calculation [19–23]. The flowchart of the GA is shown in Figure 2.

3.1. Determining Design Variables. By analyzing the structure of the reducer, we can know that the size of the planet wheel, the center wheel, and the driving wheel can greatly change the volume of the reducer. Therefore, the tooth width, modulus, and tooth number of each gear are selected as design variables, and the number of planetary gears is 4. The design variables taken in this paper are as follows:

$$X = \{x(1), x(2), x(3), x(4), x(5), x(6), x(7)\} \\ = \{b_1, m_1, z_a, z_c, b_2, m_2, z_1\}, \tag{1}$$

where b_1 and b_2 are the tooth widths of high-speed and low-speed stages, m_1 and m_2 are the moduli of high-speed and low-speed stages, z_a is the number of teeth of the sun gear, z_c is the number of planetary gears, and z_1 is the number of helical gears.

3.2. The Objective Function of the Reducer. According to the symmetrical installation condition of planet gear, concentric condition of sun gear and planet gear, and the transmission ratio formula of planetary gear train, the volume function of the reducer is as follows [19, 24]:

$$f(x) = 2f_1(x) + f_2(x) \\ = 2\pi m_1^2 b_1 \left(\frac{1}{4} z_a^2 + z_c^2 \right) + \frac{\pi}{4} m_2^2 z_1^2 b_2 \left(1 + i^2 \right). \tag{2}$$

3.3. Constraint Condition

(1) Adjacency conditions: to ensure that the planet gear does not collide, make sure there is a gap between the tips of the two planetary gears on the center line, that is, the sum of the radius of the top circle of the two adjacent planets gear should be less than the center distance.

$$d_{ac} < 2a_{ac}' \sin \frac{\pi}{4}, \tag{3}$$

where d_{ac} is the diameter of the apical circle of the planetary wheel and a_{ac}' is the center distance between the sun gear and the planet gear.

(2) The minimum number of teeth:

$$z \geq z_{\min}. \tag{4}$$

The minimum number of teeth of the sun gear in the high-speed stage of the reducer is 14–18.

(3) The minimum modulus:

$$m_1 \geq 2.86, \quad m_2 \geq 5, \tag{5}$$

where m_1 is the modulus of the planetary gear train and m_2 is the modulus of the helical gear set.

(4) Minimum tooth width:

$$b \geq 10. \tag{6}$$

(5) Coefficient of face width:

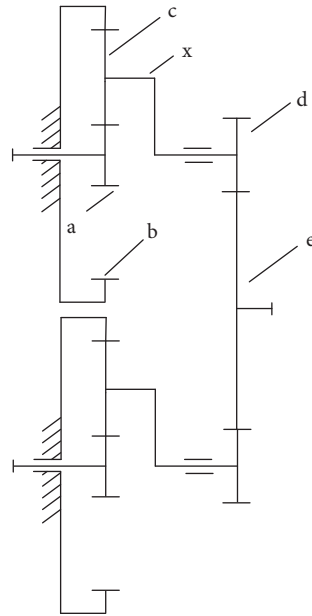FIGURE 1: Transmission diagram of reduction gearbox.

TABLE 1: Original design parameters of reducer.

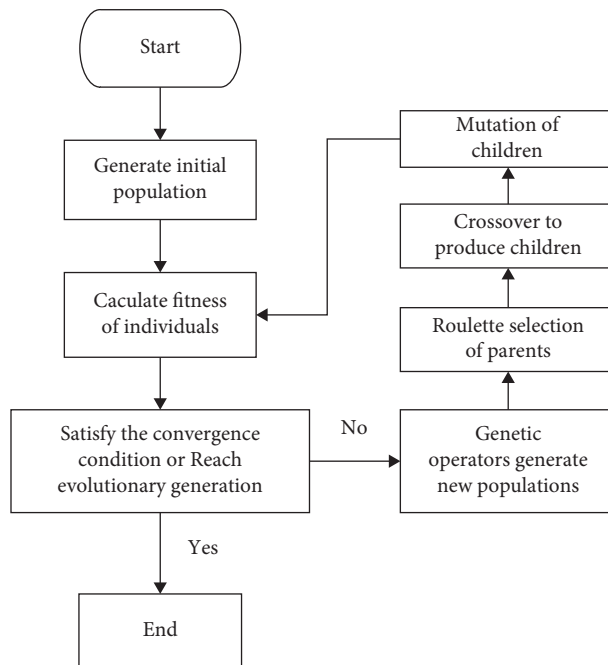| Parameter	Gear				
	Sun gear a	Planetary gear c	Ring gear b	Helical gear d	Drive gear e
m_n	3.5	3.5	3.5	7	7
Z	17	25	67	19	69
B	41	41	41	85	85
Material	20CrNi4	20CrNi4	42CrMo	20CrNi4	20CrNi4

FIGURE 2: The flowchart of the GA.

For planetary gear sets: $0.8 \leq b_1/d_a \leq 1.4$;

For the helical gear set: $1 \leq b_2/d_2 \leq 1.4$;

where b_1 is the tooth width of the planetary gear train; d_a is the diameter of the sun gear's indexing circle; b_2 is the tooth width of the helical gear set; and m_2 is the modulus of the helical gear set.

(6) Contact fatigue strength of tooth surface:

$$d_a \geq K_d \sqrt[3]{\frac{T_1 K_A K_{H\Sigma} K_{Hp}}{\phi_d \sigma_{Hlim}^2} \times \frac{u+1}{u}}, \tag{7}$$

where K_d is the coefficient of the formula. If a pair of gears is spur, then $K_d = 768$; if a pair of gears is helical, then $K_d = 720$; T_1 is the nominal torque of the pinion, $N \bullet m$; K_A is the use coefficient; u is the ratio of teeth; $K_{H\Sigma}$ is the comprehensive coefficient; K_{Hp} is the non-uniform coefficient of the load distribution of the planetary wheel when calculating the contact strength; ϕ_d is the pinion tooth width coefficient; and σ_{Hlim} is the contact fatigue strength of the gear, N/mm^2.

"In the formula, "+" is for external engagement, and "-" is for internal engagement.

(7) Bending fatigue strength of tooth root:

$$m \geq K_m \sqrt[3]{\frac{T_1 K_A K_{F\Sigma} K_{Fp} Y_{Fa1}}{\phi_d z_1^2 \sigma_{Flim}}}, \tag{8}$$

where K_m is the coefficient of calculation (in spur gear transmission, $K_m = 12.1$; in helical gear transmission, $K_m = 11.5$); $K_{F\Sigma}$ is the comprehensive coefficient; K_{Fp} is the non-uniform coefficient of load distribution between planetary wheels when calculating bending strength; z_1 is the number of pinion teeth; and σ_{Flim} is the bending fatigue strength of the test gear, N/mm^2.

(8) Assembly conditions:

$$\frac{z_a + z_b}{n_p} = C \,(\text{Integer}). \tag{9}$$

Since assembly conditions are difficult to be directly substituted in the constraint formula, they can be used as the constraint conditions to determine the number of teeth of the inner ring gear after optimization.

z_a is the number of sun gear teeth; z_b is the number of teeth of the inner ring gear; and n_p is the number of planet gears, and the value in this paper is 4.

(9) The transmission ratio error of planetary gear:

$$\left| 1 - \frac{2z_a + 2z_c}{z_a i_p} \right| - 4 \leq 0, \tag{10}$$

where i_p is the rated transmission ratio.

(10) Interference problem of the inner ring gear. As shown in Figure 3, in the process of optimizing the size, the two inner gear rings may interfere with each other because the driving gear C shrinks too much. The interference constraints of inner ring gear can be obtained as follows:

$$1.2 \leq \frac{1/2m_2 z_1 \left(1 + i_{incline}\right)}{m_1 \left(z_a + 2z_c\right)} \leq 1.4, \tag{11}$$

where $i_{incline}$ is the transmission ratio of the helical gear set.

3.4. Optimization Case Study and Optimization Result Analysis

3.4.1. Reducer Case Study. In this part, the relevant parameters of the reducer optimization design of directional drilling machine are given, the input torque is $T_{out} = 380N \bullet M$, the output torque is $T_{enter} = 7200N \bullet M$, the output speed is $n_{out} = 150r/min$, the transmission efficiency of the planetary gear is $\eta_{Row} = 0.97$, the transmission efficiency of the helical gear is $\eta_{incline} = 0.98$, and the design life of the reducer is 5~7 years.

The material used for planetary gear train is 20CrMnTi, and the hardness of the material is 217HB after carburizing and quenching treatment. The material used for the helical gear group is 20CrNi4, and the hardness of the material is 296HB after carburizing and quenching treatment. The accuracy of all the gears is 7 grade.

(1) Determination of transmission ratio at each stage: according to the original parameters of the reducer, before the optimization design, the transmission ratio of the planetary gear train is 5, and the transmission ratio of the helical gear is 3.6. Because the output torque is proportional to the transmission ratio, the output torque is sufficient while the input and output speeds meet the design objectives. Under the condition of meeting the overall layout of the reducer, the purpose of reducing the weight and saving the cost is achieved by optimizing the parameters of the reducer. According to the distribution principle of the transmission ratio of the second-level reducer, it can be known that after the transmission ratio is redistributed, the planetary gear train is $i_{Row} = 3.55$, the helical gear set is $i_{incline} = 2.8$, and the spiral angle is $10°$.

(2) Determination of input torque at each stage: in the planetary gear train, the input torque of the sun gear at each power split is as follows:

$$\begin{aligned} T_1 &= \frac{T_{enter}}{n_p} \\ &= \frac{380}{4} N \bullet M \\ &= 95N \bullet M. \end{aligned} \tag{12}$$
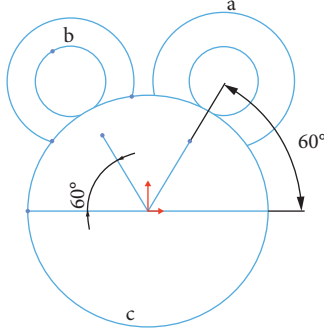
The input torque of the helical gear set is as follows:

FIGURE 3: Gear installation position diagram.

$$T_2 = T_{\text{enter}} \times i_{\text{Row}} \times \eta_{\text{Row}}$$
$$= 1308.53 N \bullet M. \tag{13}$$

(3) The allowable contact stress for high-speed gear is $[\sigma_{H1}] = 1591$MPa, allowable bending stress of tooth root is $[\sigma_{F1}] = 346.5$MPa, the allowable contact stress of the tooth surface of the low-speed gear is $[\sigma_{H2}] = 1295$MPa, and the allowable bending stress of the tooth root is $[\sigma_{F2}] = 443.52$MPa.

Put the above parameters into the constraint condition, and the constraint function is as follows [25]:

$$c_1(x) = -\frac{\sqrt{2}}{2}z_a + \frac{2-\sqrt{2}}{2}z_c < -2,$$

$$c_2(x) = 0.8m_1 z_a - b_1 \leq 0,$$

$$c_3(x) = b_1 - 1.4m_1 z_a \leq 0,$$

$$c_4(x) = m_2 z_1 - b_2 \leq 0,$$

$$c_5(x) = b_2 - 1.4m_2 z_1 \leq 0,$$

$$c_6(x) = 88382.7765 \times \frac{z_a + z_c}{b_1 z_c} - m_1^2 z_a^2 \leq 0,$$

$$c_7(x) = 549047.233 \times \frac{1}{b_2} - m_2^2 z_1^2 \leq 0, \tag{14}$$

$$c_8(x) = 7335.3088 \times \frac{1}{b_1 z_a} - m_1^2 \leq 0,$$

$$c_9(x) = 27675.4 \times \frac{1}{b_2 z_1} - m_2^2 \leq 0,$$

$$c_{10}(x) = \left| 1 - \frac{2z_a + 2z_c}{z_a i_p} \right| - 4\% \leq 0,$$

$$c_{11}(x) = 1.2m_1 (z_a + 2z_c) - \frac{1}{2}m_2 z_1 (1 + i_{\text{incline}}) \leq 0,$$

$$c_{12}(x) = \frac{1}{2}m_2 z_1 (1 + i_{\text{incline}}) - 1.4m_1 (z_a + 2z_c) \leq 0.$$

3.4.2. Optimization Design and Result Analysis. In this study, the optimization problem belongs to the optimization solution of the single-objective function nonlinear constraint minimization problem [26]. By using the MATLAB genetic algorithm toolbox, users only need to input the number of variables, the upper and lower limits of constraint values, the file name of fitness function M, and file name of constraint condition function M on the interface and set the population size, crossover probability, and mutation probability to calculate the optimal value [27, 28]. The specific steps are as follows:

(1) Write the M file for the fitness function, as shown in Figure 4.

(2) Write the M file of the constraints, as shown in Figure 5.

(3) Use the genetic algorithm toolbox of MATLAB to call the written fitness function M file and constraint condition function M file and input the number of variables, the corresponding linear constraint value, and boundary, as shown in Figure 6. The crossover probability is 0.6, the mutation probability is 0.08, and the other parameters are the default parameters of the system.

After the setting is complete, click Start to run, and the running result is shown in Figure 7.

Since the number of teeth and moduli are discrete variables, the results should be rounded, and the rounded design variables should be substituted into the constraint conditions to verify that they meet the requirements [29]. The comparison between the final parameters and the original data is as follows.

Table 2 shows that the volume of the reducer optimized by the genetic algorithm is reduced by 49.6% compared with the original volume. The optimized reducer has a smaller volume, a more compact structure, and saves materials. Finally, the optimization goal is achieved.

4. Transient Dynamics Analysis of the Reducer

In this part, to verify the reliability of the optimized reducer, transient dynamics analysis of the planetary gear set and helical gear set in the reducer was carried out by using ANSYS Workbench.

4.1. Transient Dynamics Equation. Transient dynamics analysis is a method used to determine the dynamic response of a structure under any time-varying load. By transient dynamics analysis, the time-varying displacements, forces, stresses, and strains of the structure under the random combination of transient, steady, and harmonic loads can be determined [30].

The basic equation of motion for transient dynamics is as follows:

$$M\ddot{u} + C\dot{u} + Ku = F(t), \tag{15}$$

FIGURE 4: M file of the objective function.

FIGURE 5: M files for constraints.
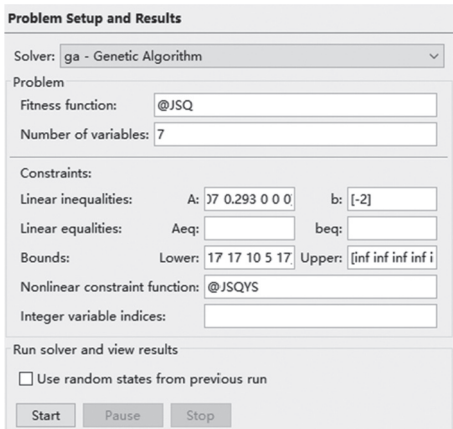
FIGURE 6: Genetic algorithm toolbox interface.

FIGURE 7: Optimization results of genetic algorithm.

where M is the mass matrix; C is the damping matrix; K is stiffness matrix; $\ddot{u}$ is nodal acceleration vector; $\dot{u}$ is node velocity vector; and u is the node displacement vector.

4.2. The Establishment of Finite Element Model. The optimized gear was modeled by Creo, and then the finite element model of planetary gear and helical gear was obtained, as shown in Figures 8(a) and 8(b). Save the 3D model as .STP format.

4.3. Establishment of the Transient Dynamics Model

4.3.1. Definition of Gear Material. The transient structure was opened in ANSYS Workbench, and the 3D model of the gears was imported into ANSYS Workbench for analysis, and its material properties were defined. 20CrMnTi is used for both the sun wheel and the planet wheel, 42CrMo is used for the inner gear ring, and 20CrNi4 is used for the helical gear set. The material properties are shown in Table 3 [31].

4.3.2. Finite Element Mesh Determination of Gears. The gear model was imported, tetrahedral mesh was adopted, 1/3 of the minimum side length of the gear was taken as the minimum mesh size to divide, and the medium smoothing method was considered. Sizing command was used to control the mesh size of 3 mm in planetary gear train, and contact sizing command was added to encrypt the mesh of the contact region of the gear, and the mesh size was 1 mm. Sizing command was used to control the mesh unit size of 5 mm in the helical gear group, and contact sizing command was added to encrypt the mesh in the contact region of the gear, and the mesh size was 2 mm. After setting, the mesh will be generated, and the average quality of the mesh should be controlled above 0.7 [32]. The contact problem of gears is a highly nonlinear behavior, which requires a lot of computing resources. In order to improve the operation efficiency, reduce the amount of computer calculation, minimize the size of the model on the premise of satisfying the calculation accuracy, and ensure that it is close to the actual working conditions, and the model in Creo needs to be simplified. In the planetary gear train, because there are four planetary gears in contact with the sun gear, the load on each planetary gear is uniform. Therefore, you only need to analyze and calculate one group. In the helical gear set, only the gear meshing part is kept for analysis and calculation. Generated finite element meshes are presented in Figure 9 [33, 34].

4.3.3. Boundary Conditions and Load Conditions. Boundary conditions in planetary gear train include frictionless contact between solar gear and planetary gear, as shown in Figure 10(a); frictionless contact between planetary gear and inner ring gear, as shown in Figure10(b); the rotation pair between the planetary frame and the planetary wheel, as shown in Figure 11(a); the rotation pair of the solar wheel to the earth, as shown in Figure 11(b); the rotation pair of the planetary frame to the earth, as shown in Figure 11(c); and the fixed pair of the inner ring to the ground, as shown in Figure 12.

In the helical gear set, the boundary conditions include frictionless contact pairs of the pinion and the large gear and rotation pairs of the two gears against the ground, as shown in Figure 13 [35].

In the planetary gear train, the sun gear is chosen as the driving wheel, and the load is applied to the sun gear in the form of torque, and the planet rack is the output. In the helical gear, the pinion is selected as the driving gear, and the load is also applied to the pinion in the form of torque.

TABLE 2: Comparison of reducer parameters before and after optimization.

| Parameters	Results before optimization					Results after optimization				
	Sun gear	Ring gear	Planetary gear	Helical gear	Drive gear	Sun gear	Ring gear	Planetary gear	Helical gear	Drive gear
m (mm)	3.5	3.5	3.5	7	7	3	3	3	5	5
z	17	67	25	19	69	23	57	17	21	59
b (mm)	41	41	41	85	85	68	68	68	103	103
Material	20CrNi4	42CrMo	20CrNi4	20CrNi4	20CrNi4	20CrMnTi	42CrMo	20CrMnTi	20CrNi4	20CrNi4
Volume (mm³)			18945724.2					9546848.15		
Volume decrease ratio					49.6%					

(a)

(b)
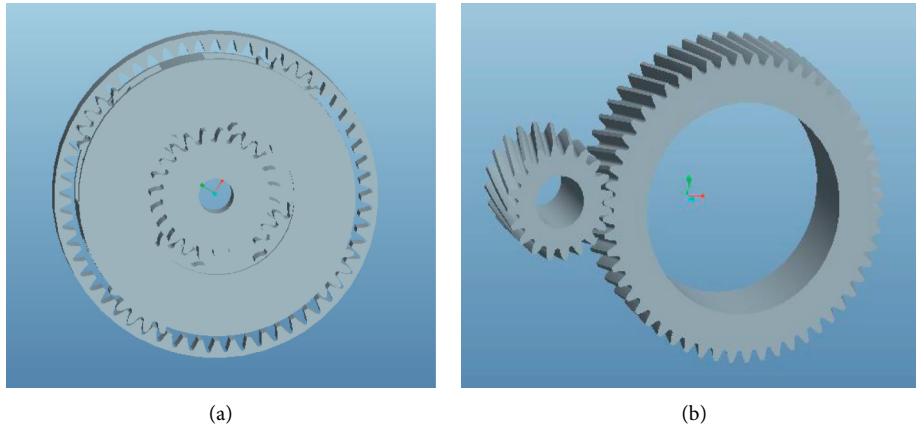
FIGURE 8: .3D model of gears. (a) 3D model of planetary gear. (b) 3D model of helical gear.

TABLE 3: Material properties of gears.

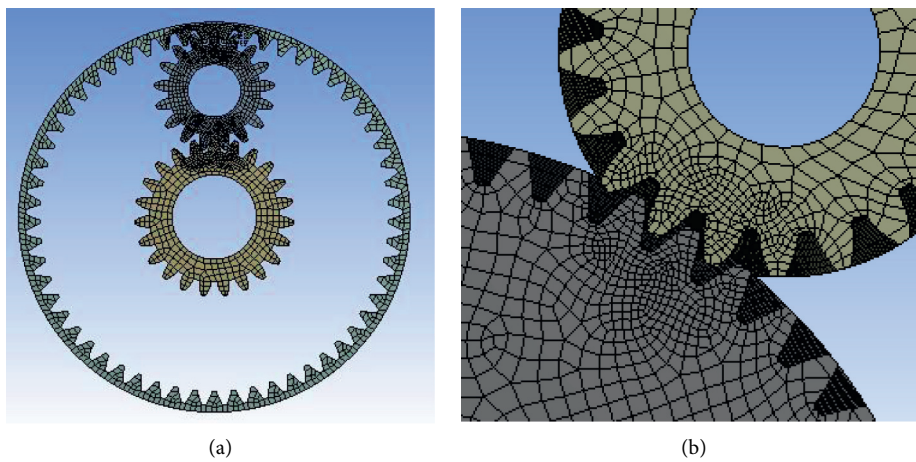| No.	Property	20CrMnTi	42CrMo	20CrNi4
1	Density (Kg/m³)	7800	7850	7800
2	Poisson's ratio	0.25	0.26	0.29
3	Young's modulus (Pa)	2.07 E+11	2.21 E+11	2.07 E+11

(a)

(b)

FIGURE 9: Finite element mesh of gears. (a) Planetary gear. (b) Helical gears.
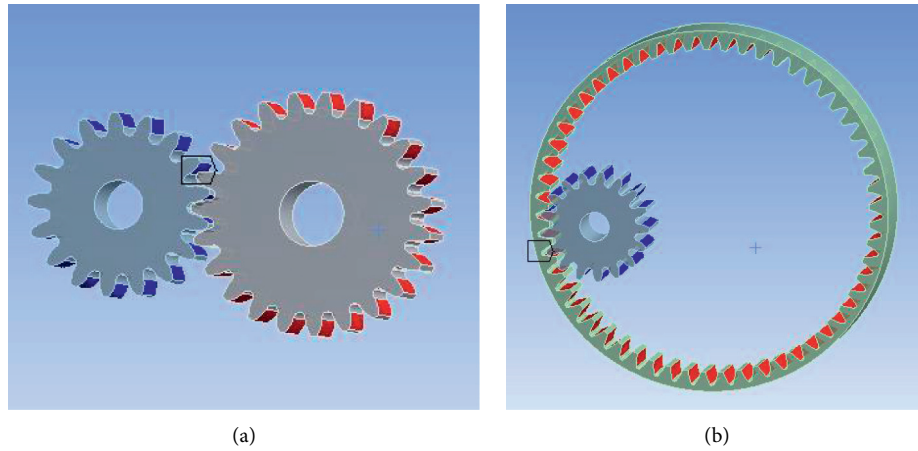
(a)

(b)

FIGURE 10: Friction contact pairs in a planetary gear train. (a) The contact pair between the sun gear and the planetary gear. (b) Contact pair of planetary gear and inner ring gear.
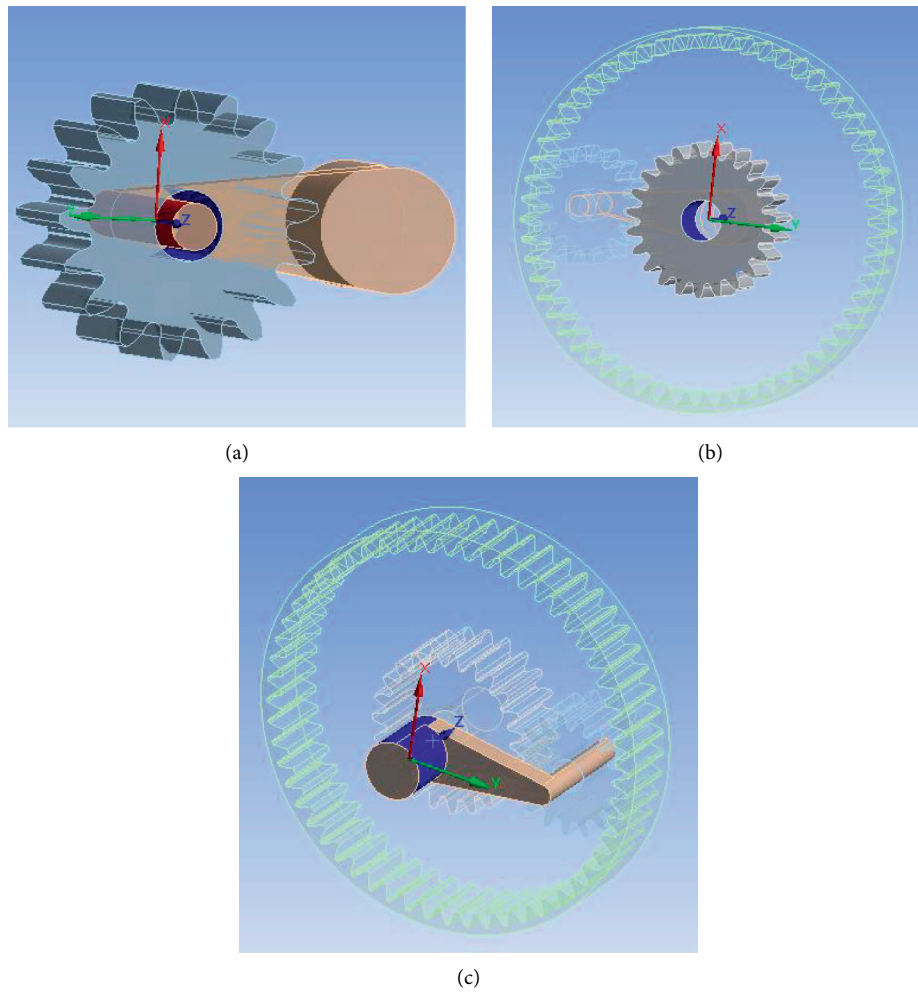

(a)

(b)

(c)

FIGURE 11: Rotation pairs in planetary gear system. (a) Rotation pairs between planet carrier and planetary gear. (b) Rotation pairs between sun gear and earth. (c) Rotation pairs between planet carrier and earth.
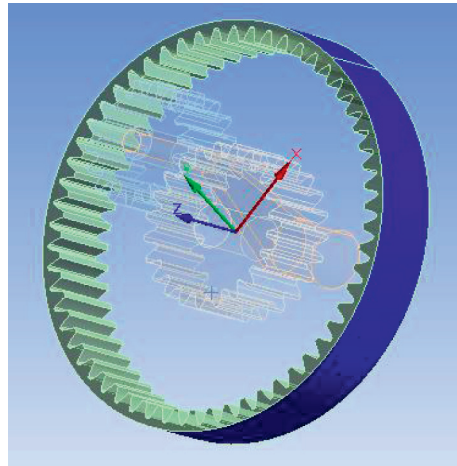
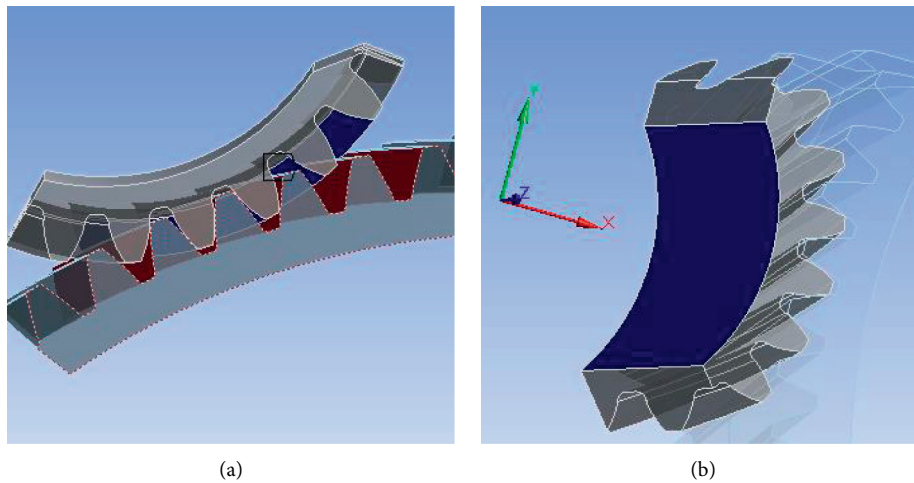FIGURE 12: Fixed pair of inner gear ring to ground.

(a)   (b)

FIGURE 13: Boundary conditions of helical gears. (a) Helical gear contact pair. (b) The ground pair of helical gears.

A: Transient Structural
Total Deformation
Type: Total Deformation
Unit: mm
Time: 1
2021/11/6 21:56

0.13639 Max
0.12124
0.10608
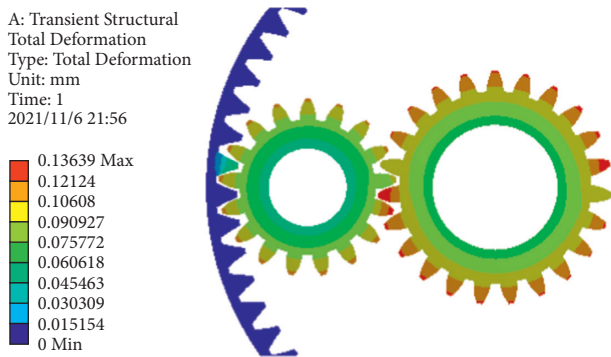0.090927
0.075772
0.060618
0.045463
0.030309
0.015154
0 Min

FIGURE 14: Deformation program of the planetary gear train.

5. Transient Dynamics Analysis Results and Discussion

According to the above settings, the total deformation program, equivalent stress program, and equivalent strain program of the gear train are obtained after transient dynamics analysis of the gear train, as shown in Figures 14–21 [36, 37]. Since the maximum strain and stress in the planetary gear train occur in the sun gear, only the stress and strain on the sun gear are analyzed.

Table 4 shows the output response of transient dynamics analysis, and Table 5 shows the maximum output response of each contact pair in the reducer gear train.

As shown in Figures 13–15, the maximum deformation in the planetary gear train occurs at the edge of the sun gear tooth, and the maximum deformation is 0.1364 mm. Both the maximum strain and the maximum stress appear near the node line of the sun gear. The maximum strain is 0.01161, and the maximum stress is 705.67 MPa. As shown in Figures 17 and 18, the maximum deformation of the helical gear group appears at the edge of the helical gear, and the maximum deformation is 0.7974 mm. The maximum strain and maximum stress both appear near the pitch line of the helical gear, and the maximum strain is 2.4692 and the maximum stress is 478.23 MPa [33, 38].

Figures 16 and 20 show the stress diagrams of the planetary gear train and the helical gear group. The root
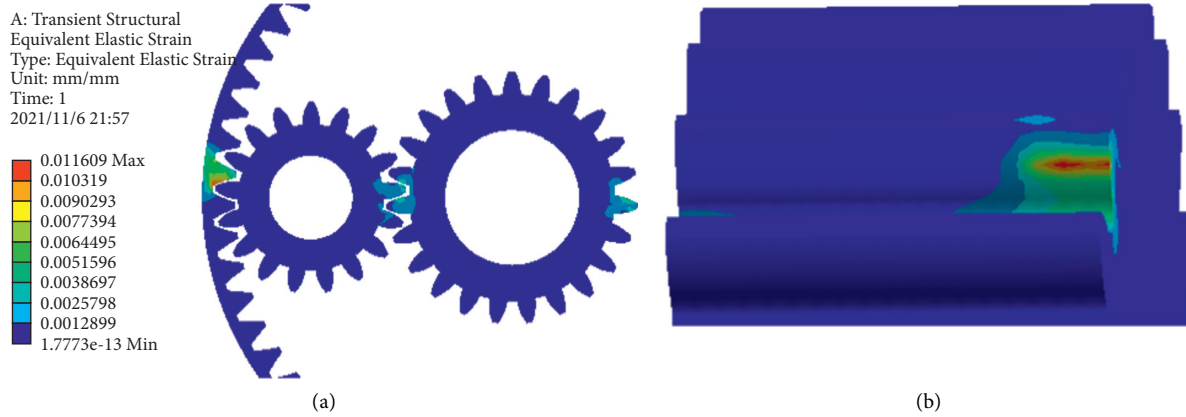
FIGURE 15: Equivalent strain program of the planetary gear train. (a) Equivalent strain program. (b) Program of sun gear strain.
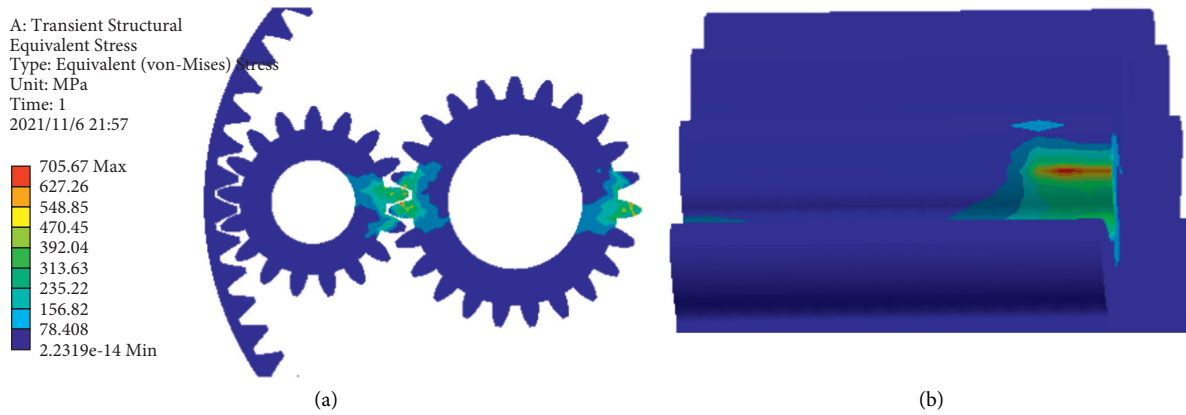

FIGURE 16: Program of equivalent stress of the planetary gear train. (a) Equivalent stress program. (b) Program of sun gear stress.
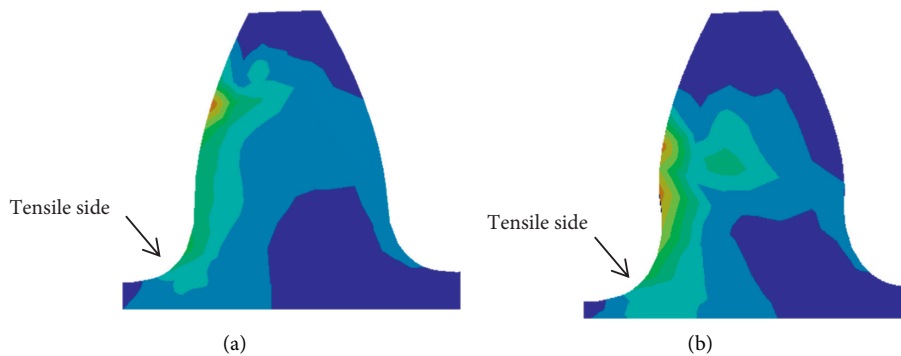
FIGURE 17: Root stress of the planetary gear train. (a) Root stress cloud of the sun gear. (b) Root stress cloud of the planetary gear.

stress on the tensile side is the key factor leading to tooth failure, so the stress on the tensile side is mainly considered [39]. In the planetary gear train, the stress value of the teeth root radius on the tensile side of the sun gear and the planet gear is 393.84 MPa and 472.61 MPa, respectively, which is less than the yield limit of the materials. In the helical gear set, the root stress on the tensile side of the two gears is about 288.3 MPa. It is also less than the yield limit of the materials.

A: Transient Structural
Total Deformation
Type: Total Deformation
Unit: m
Time: 1
2021/7/22 0:19

0.00079741 Max
0.00077668
0.00075595
0.00073522
0.00071449
0.00069376
0.00067303
0.0006523
0.00063157
0.00061084 Min

FIGURE 18: Deformation nephogram of helical gear set.

A: Transient Structural
Equivalent Elastic Strain
Type: Equivalent Elastic Strain
Unit: m/m
Time: 1
2021/7/22 0:20

0.0024692 Max
0.0021948
0.0019205
0.0016461
0.0013718
0.0010974
0.00082305
0.0005487
0.00027435
3.5324e-9 Min

(a)

(b)

FIGURE 19: Equivalent strain program of the helical gear group. (a) Equivalent strain program. (b) Strain program of helical gear.

A: Transient Structural
Equivalent Stress
Type: Equivalent (von-Mises) Stress
Unit: Pa
Time: 1
2021/7/22 0:22

4.7823e8 Max
4.2509e8
3.7196e8
3.1882e8
2.6568e8
2.1255e8
1.5941e8
1.0627e8
5.3137e7
481.27 Min

(a)

(b)

FIGURE 20: Equivalent stress nephogram of the helical gear group. (a) Equivalent stress nephogram. (b) Stress nephogram of helical gear.

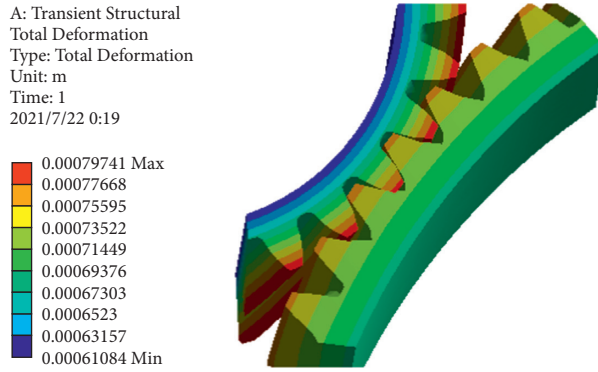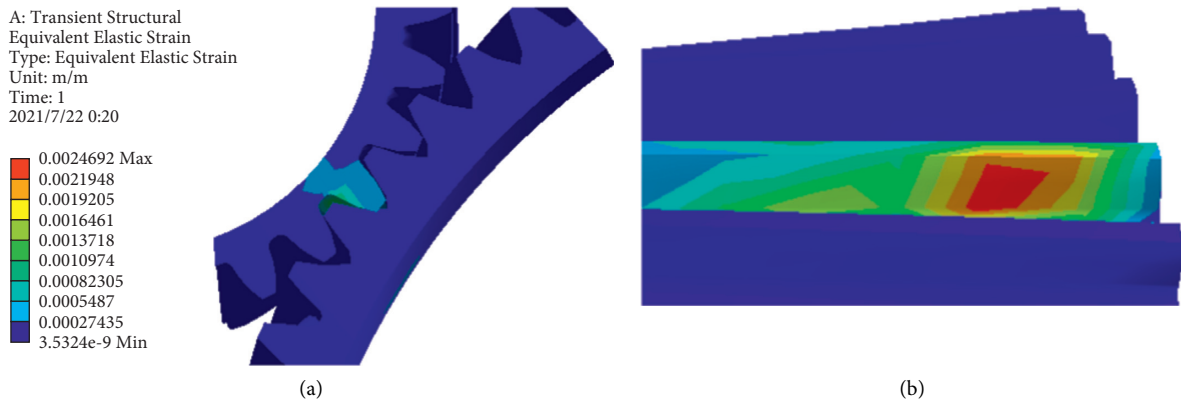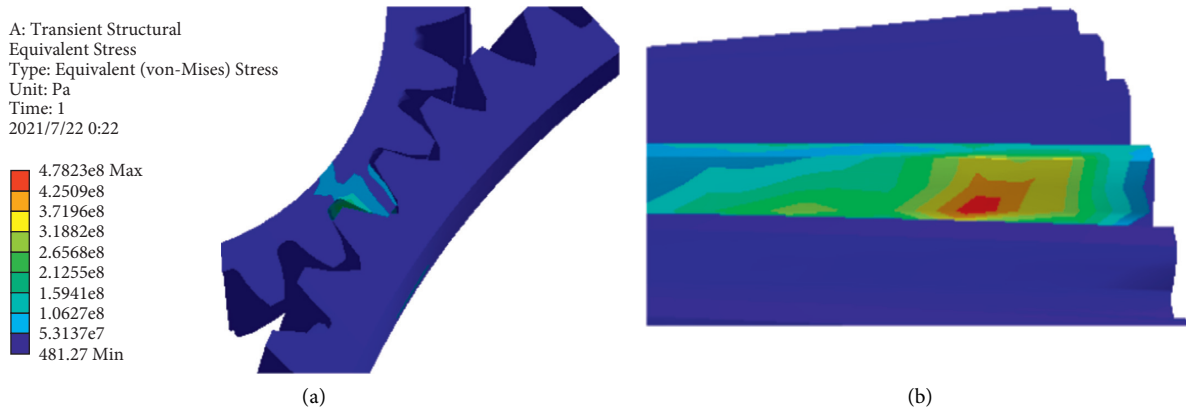(a)   (b)
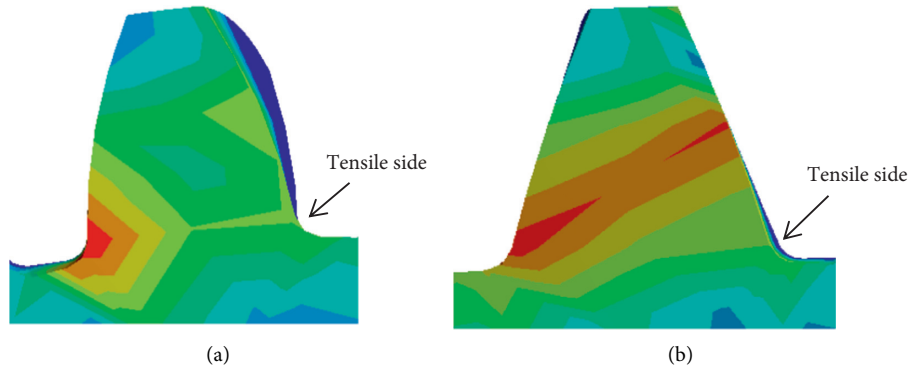
FIGURE 21: Root stress of the helical gear group. (a) Root stress cloud of the helical gear. (b) Root stress cloud of the drive gear.

TABLE 4: Output response of finite element analysis.

No.	Output characteristics	Symbol	SI unit
1	Total deformation	R1	mm
2	Equivalent elastic strain	R2	—
3	Equivalent von Mises stress	R3	MPa

TABLE 5: Maximum results of finite element analysis.

Output variable	Sun gear-planetary gear	Planetary gear-internal gear	Helical gear
R1	0.1364	0.0909	0.79741
R2	0.01161	0.00516	0.0024692
R3	705.67	306.82	478.23

6. Conclusion

In this paper, MATLAB genetic algorithm is used to carry out a lightweight design for the directional drilling gear reducer, and the optimized gear parameters are obtained. Through calculation, the volume of the optimized model is reduced by 49.6% compared with the original gear model, achieving the purpose of being lightweight (Figure 21).

Three-dimensional modeling software was used to model the optimized gear, and transient dynamics analysis of planetary gear set and helical gear set was carried out with ANSYS Workbench. Through analysis, we can obtain the convergent force curve the convergent displacement curve and the response cloud graph. Through analysis, the maximum stress and strain appear on the contact line of gear meshing. The maximum stress is less than the yield limit of the sun gear material, and the maximum strain is less than the elongation and section shrinkage of the sun gear material. In the helical gear group, the maximum stress and strain also appear on the contact line of gear meshing, and the maximum stress value is less than the yield limit of the helical gear material, and the maximum strain value is less than the elongation and section shrinkage of the helical gear material. Therefore, the optimized gear meets the strength requirements and achieves the purpose of being lightweight.

Data Availability

The data used to support the findings of this study are included within the article.

Conflicts of Interest

The authors declare that there are no conflicts of interest regarding the publication of this article.

Acknowledgments

References

[1] F. R. Patino, C. Layhee, and C. Arson, "Horizontal directional drilling (HDD) alignment optimization using ant colony optimization," *Tunnelling and Underground Space Technology*, vol. 103, Article ID 103450, 2020.

[2] H. Li, Y. Liu, and W. Wang, "The integrated drainage technique of directional high-level borehole of super large diameter on roof replacing roof extraction roadway: a case study of the underground zhaozhuang coal mine," *Energy Report*, vol. 6, pp. 2651–2666, 2020.

[3] H. Lu, T. Iseley, J. Matthews, and W. Liao, "Hybrid machine learning for pullback force forecasting during horizontal directional drilling," *Automation in Construction*, vol. 129, Article ID 103810, 2021.

[4] Y. Wang, "Status and prospect of gas drainage technology and equipment in Coal mines in China," *Safety In Coal Mines*, vol. 51, no. 10, pp. 67–77, 2020, In chinese.

[5] S. Zhang, *Strategic Thinking of the 13th Five-Year Plan of CBM Industry*, China Electric Power News, Chin, pp. 6–13, 2015, In chinese.

[6] F. Mu, X. Zhao, L. Wu et al., "China coal seam gas industry operation rules and improvement," *China Mining Industry*, vol. 25, no. 8, pp. 1–4, 2016, In Chinese.

[7] Y. Ningping, Z. Jie, J. Xing, and H. Hanjing, "Status and development of directional drilling technology in coal mine," *Procedia Engineering*, vol. 73, pp. 289–298, 2014.

[8] X. Yan, S. T. Ariaratnam, S. Dong, and C. Zeng, "Horizontal directional drilling: state-of-the-art review of theory and applications," *Tunnelling and Underground Space Technology*, vol. 72, pp. 162–173, 2018.

[9] R. Ramadani, S. Pal, M. Kegl et al., "Topology optimization and additive manufacturing in producing lightweight and low vibration gear body," *International Journal of Advanced Manufacturing Technology*, vol. 113, no. 11, pp. 3389–3399, 2021.

[10] G. Madhusudan and C. Vijayasimha, "Approach to spur gear design," *Computer-Aided Design*, vol. 19, no. 10, pp. 555–559, 1987.

[11] D. F. Thompson, S. Gupta, and A. Shukla, "Tradeoff analysis in minimum volume design of multi-stage spur gear reduction units[J]," *Mechanism and Machine Theory*, vol. 35, no. 5, pp. 609–627, 2000.

[12] P. Rai, A. Agrawal, and B. G. Asim, "Volume optimization of helical gear with profile shift using real coded genetic algorithm," *Procedia Computer Science*, vol. 133, pp. 718–724, 2018.

[13] S. Vinoth, S. Nandhini, and K. Pavithra, "Relative study on concrete filled square and circular steel tubular columns – using ANSYS for mathematical analysis," *Materials Today: Proceedings*, vol. 47, pp. 6060–6066, 2021.

[14] J. Naranjo, V. Miguel, and J. Coello, "Analysis and simulation of single point incremental forming by ANSYS®," *Procedia Engineering*, vol. 132, 2015.

[15] M. P. Jenarthanan, K. S. Ramesh, and S. Nishanthan, "Analysis of leaf spring using Carbon/Glass Epoxy and EN45 using ANSYS: a comparison," *Materials Today: Proceedings*, vol. 5, no. 6, Article ID 14519, 2018.

[16] C. Razvan, G. Lucian, and M. Ioan, "An oop Matlab extensible framework for the implementation of genetic algorithms. Part I: the framework," *Procedia Technology*, vol. 19, pp. 193–200, 2015.

[17] J. Yang, "Indoor space compositions based on genetic algorithms to optimize neural networks," *Physical Communication*, vol. 42, Article ID 101167, 2020.

[18] A. J. Santhosh, A. D. Tura, I. T. Jiregna, W. F. Gemechu, N. Ashok, and M. Ponnusamy, "Optimization of cnc turning parameters using face centred ccd approach in rsm and ann-genetic algorithm for aisi 4340 alloy steel," *Results in Engineering*, vol. 11, Article ID 100251, 2021.

[19] V. Savsani, R. Rao, and D. Vakharia, "Optimal weight design of a gear train using particle swarm optimization and simulated annealing algorithms," *Mechanism and Machine Theory*, vol. 45, no. 3, pp. 531–541, 2010.

[20] S. Papadamou and G. Stephanides, "Improving technical trading systems by using a new matlab-based genetic algorithm procedure," *Mathematical and Computer Modelling*, vol. 46, no. 1, pp. 189–197, 2007.

[21] J. G. B. Rueda and A. Guzmán, "Genetic algorithm model and data files to assess jonswap spectra coefficients: Matlab code," *Data in Brief*, vol. 32, Article ID 106196, 2020.

[22] V. Consonni, G. Baccolo, F. Gosetti, R. Todeschini, and D. Ballabio, "A Matlab toolbox for multivariate regression coupled with variable selection," *Chemometrics and Intelligent Laboratory Systems*, vol. 213, Article ID 104313, 2021.

[23] V. Panwar, D. S. Kumar, K. K. Pradeep, A. Jain, and C. Thakar, "Experimental investigations and optimization of surface roughness in turning of en 36 alloy steel using response surface methodology and genetic algorithm," *Materials Today: Proceedings*, vol. 46, pp. 6474–6481, 2021.

[24] C. Wang, "Multi-objective optimal design of modification for helical gear," *Mechanical Systems and Signal Processing*, vol. 157, Article ID 107762, 2021.

[25] Y. Kan, D. Sun, Y. Luo, D. Qin, J. Shi, and K. Ma, "Optimal design of the gear ratio of a power reflux hydraulic transmission system based on data mining," *Mechanism and Machine Theory*, vol. 142, Article ID 103600, 2019.

[26] T. Yokota, T. Taguchi, and M. Gen, "A solution method for optimal weight design problem of the gear using genetic algorithms," *Computers & Industrial Engineering*, vol. 35, no. 3, pp. 523–526, 1998.

[27] Da Cui, G. Wang, and K. Sun, "Reliability design and optimization of the planetary gear by a GA based on the DEM and Kriging model," *Reliability Engineering & System Safety*, vol. 203, 2020.

[28] D. Adanza, V. Moreno, and G. Génova, "An automatic methodology for the quality enhancement of requirements using genetic algorithms," *Information and Software Technology*, vol. 140, Article ID 106696, 2021.

[29] P. N. E. Naveen, M. M. Chaitanya, and R. K. R. M. Raghu, "Design and optimization of nylon 66 reinforced composite gears using genetic algorithm," *Materials Today: Proceedings*, vol. 46, 2021.

[30] G. Dong and P. Chen, "The vibration characteristics of drillstring with positive displacement motor in compound drilling Part 2: transient dynamics and bit control force analysis," *International Journal of Hydrogen Energy*, vol. 43, no. 27, Article ID 12199, 2018.

[31] A. Kumar and P. P. Patil, "FEA simulation and RSM based parametric optimisation of vibrating transmission gearbox housing," *Perspectives in Science*, vol. 8, 2016.

[32] M. Domenico, P. Antonio, and S. Shadi, "A study on the dynamic behaviour of lightweight gears," *Shock and Vibration*, vol. 2017, Article ID 7982170, 12 pages, 2017.

[33] X. Qi and X. Shen, "Multidisciplinary design optimization of turbine disks based on ANSYS Workbench platforms," *Procedia Engineering*, vol. 99, 2015.

[34] M. Batsch, "Mathematical model and tooth contact analysis of convexo-concave helical bevel novikov gear mesh[J]," *Mechanism and Machine Theory*, vol. 149, Article ID 103842, 2020.

[35] A. C. R Kumar, R. N. Mohammed, and S. Selvakumar, "Static structural analysis of spur gear using ANSYS 15.0 and material selection by COPRAS, MOORA techniques," *Materials Today: Proceedings*, vol. 47, pp. 25–36, 2021.

[36] S. Chavadaki, K. K. Nithin, and M. Rajesh, "Finite element analysis of spur gear to find out the optimum root radius," *Materials Today: Proceedings*, vol. 46, Article ID 10675, 2021.

[37] S. Avikal, A. Bisht, D. Sharma et al., "Design and fatigue analysis of front axle beam of a heavy duty truck using Ansys," *Materials Today: Proceedings*, vol. 26, pp. 3211–3215, 2020.

[38] R. Gukendran, M. Sambathkumar, C. Sabari, C. R. R. Ranjith, and V. K. Ranjeeth, "Structural analysis of composite wind turbine blade using Ansys," *Materials Today: Proceedings*, 2021.

[39] T. G. Yılmaz, O. Doğan, and F. Karpat, "A comparative numerical study of forged Bi-metal gears: bending strength and dynamic response," *Mechanism and Machine Theory*, vol. 141, pp. 117–135, 2019.